V/f controlled Virtual PM Machine for Grid-connected Inverter

Preferred Topic 1: Topic 4 – MEASUREMENT, SUPERVISION AND CONTROL FOR POWER CONVERTERS
Preferred Subtopic 1: Subtopic 4b – Standard and Advanced Current / Voltage / Synchronization Control Techniques
Preferred Topic 2: Topic 9 – POWER SUPPLIES AND INDUSTRY-SPECIFIC APPLICATIONS
Preferred Subtopic 2: Subtopic 9f – Distributed Power Supplies

Origin: University

Preference: Dialogue Session

Keywords

«DC-AC», «DC-AC converter», «Grid-connected inverter», «Voltage control»

Abstract

The paper discusses a V/f controlled virtual PM machine. The state equation of virtual PM machine is approximated to second-order system. The output power response is evaluated by the comparison to the second-order system. The response is checked by the simulations.

Introduction

Recently, the technics for a high-performance motor drive and high-efficiency motors have been actively studied and developed due to the energy conservation. Especially, permanent magnet synchronous motors (PMSM) is used because it is efficient. In the control for PMSM, the current control by a field oriented control (FOC) is known as an efficient control. The FOC requires the rotor position sensor for a detection of the magnet pole position. However, using the position sensor causes an increasing a cost of motor drive systems. Also, it is difficult to apply the position sensors to high-speed motors. Hence, a sensorless FOC is commonly used for the PMSM driver. The sensorless FOC estimates the magnetic pole position. However, the estimation requires a high-performance digital signal processor. Thus, a V/f control is proposed for the control of PMSM with a simple speed control.

In this paragraph, the application of the motor drive technic to the grid-connection system is described. The grid-connection system has similarities with the PMSM drive system. For example, inductance, resistance and a induced voltage that included PMSM is considered to the circuit elements of the grid-connection system.

This paper discusses about V/f controlled virtual PMSM for a grid-connected system. The proposed V/f control is fixed for a grid-connected inverter. The V/f control outputs the inverter voltage according to rotation speed. However, the speed control is impossible by the V/f control because the grid angular frequency is not generally determined by the inverter voltage. Thus, a virtual PMSM is used to the speed control for synchronous to the grid. The virtual load is used in the V/f control because the output torque of PMSM is determined by a load torque and the speed is generally constant. As a result, the V/f controlled PMSM is the output power controller. The output power control response is evaluated by the comparison with the approximated low-order system.

V/f control for grid-connected inverter

A. Comparison between PMSM and grid-connection

Figure 1 shows a circuit diagram of the grid-connection. Comparing the elements of this grid-connection system and the PMSM, the wiring resistance R corresponds to the winding resistance, the grid-tied inductance L corresponds to the armature inductance, and the grid voltage corresponds to the induced voltage. In addition, the voltage equation is same as the surface PMSM (SPMSM) because d-axis inductance and q-axis inductance are equal. In the other hand, the grid-connection system does not include a load torque and a moment of inertia. Also, the grid frequency corresponding to a electric frequency of PMSM is uncontrollable. Thus, the rotation speed is also uncontrollable. However, the output power

control of the grid-connection system is possible by reproducing the load torque and the moment of the inertia with a controller.

B. V/f control

Generally, PMSM control uses the dq-axis Cartesian coordinate system with the d-axis defined as the direction of the PM flux and the q-axis defined as the direction of the induced voltage. In this paper, the q-axis defined as the direction of the grid voltage to apply the V/f control for the grid-connection. The proposed control principle is based on the V/f control with the stabilization control [1]-[4], which has been proposed for PMSM. The V/f control uses the γδ-axis Cartesian coordinate system with the γ-axis defined as the direction of the inverter output voltage and the δ-axis defined as the direction 90 degrees behind the γ-axis.

Figure 2 shows the relationship between the dq-axis coordinate and the γδ-axis coordinate. The voltage equation of PMSM in the dp-axis coordinate is expressed as in (1),

$$\begin{bmatrix} v_d \\ v_q \end{bmatrix} = \begin{bmatrix} R+pL & -\omega L \\ \omega L & R+pL \end{bmatrix} \begin{bmatrix} i_d \\ i_q \end{bmatrix} + \begin{bmatrix} 0 \\ \omega \psi_m \end{bmatrix} \quad (1),$$

where R is the winding resistance, L is the armature inductance, p is the differential operator, Ψ_m is the flux linkage by PM, ω is the electric angular frequency. The grid-voltage agrees the q-axis voltage v_q in the grid-connection with a no-load condition. Thus, the virtual flux linkage of the grid-connection is expressed as in (2),

$$\psi_m = \frac{V_{grid}}{\sqrt{2}\omega_{grid}} \quad (2),$$

where V_{grid} is the maximum grid line-to-line voltage, ω_{grid} is the grid angular frequency. The voltage equation and the output power equation of grid-connection in the γδ-axis coordinate are expressed as in (3) and (4), respectively,

$$\begin{bmatrix} v_\gamma \\ v_\delta \end{bmatrix} = \begin{bmatrix} R+pL & -\omega_{grid}L \\ \omega_{grid}L & R+pL \end{bmatrix} \begin{bmatrix} i_\gamma \\ i_\delta \end{bmatrix} + \frac{V_{grid}}{\sqrt{2}} \begin{bmatrix} \sin\delta \\ \cos\delta \end{bmatrix} \quad (3),$$

$$P_{out} = \frac{V_{grid} i_q}{\sqrt{2}} = \frac{V_{grid}\left(i_\gamma \sin\delta + i_\delta \cos\delta\right)}{\sqrt{2}} \quad (4),$$

where δ is the deviation angle between γδ-axis coordinate and dq-axis coordinate, P_{out} is the output power.

The state equation of PMSM is derived by performing a linear approximation near the steady-state in the same way as Ref. [1]-[4], and expressed as in (5),

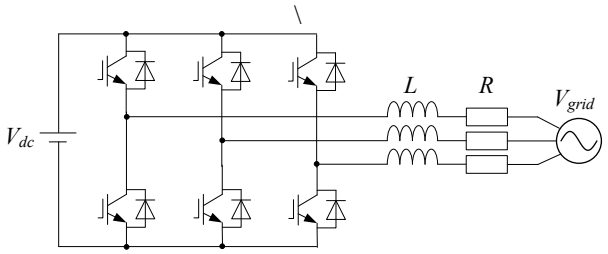

Fig. 1. The circuit configuration of the grid-connected inverter.

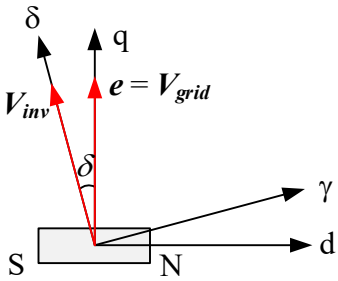

Fig. 2.The relationship between the dq-axis coordinate and γδ-axis coordinate.

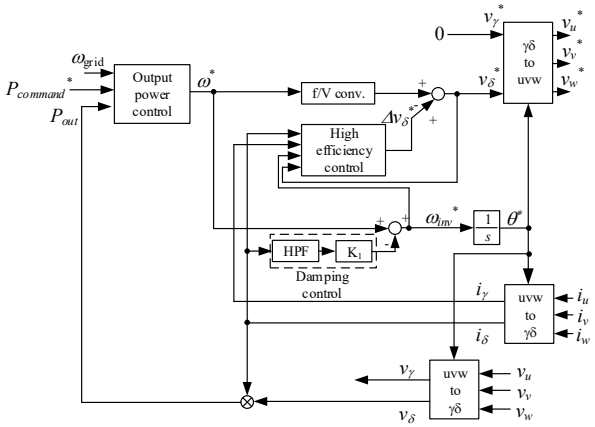

Fig. 3. The control diagram of the proposed V/f control for the grid-connection system.

$$p\mathbf{x} = \mathbf{A}\mathbf{x} + \mathbf{B}\mathbf{u} \quad (5),$$

where $\mathbf{x} = {}^t\left[\Delta i_\gamma \quad \Delta i_\delta \quad \Delta\omega \quad \Delta\delta\right]$, $\mathbf{u} = {}^t\left[\Delta v_\gamma \quad \Delta v_\delta \quad \Delta\omega_{inv}\right]$,

$$\mathbf{A} = \begin{bmatrix} -\frac{R}{L} & \omega_0 & -\frac{\psi_m}{L}\sin\delta_0 & -\frac{\psi_m}{L}\cos\delta_0 \\ -\omega_0 & -\frac{R}{L} & -\frac{\psi_m}{L}\cos\delta_0 & \frac{\psi_m}{L}\sin\delta_0 \\ \frac{P_f^2\psi_m}{J}\sin\delta_0 & \frac{P_f^2\psi_m}{J}\cos\delta_0 & 0 & \frac{P_f^2\psi_m}{J}\left(i_{\gamma 0}\sin\delta_0 + i_{\delta 0}\cos\delta_0\right) \\ 0 & 0 & -1 & 0 \end{bmatrix},$$

$$\mathbf{B} = \begin{bmatrix} \frac{1}{L} & 0 & i_{\delta 0} \\ 0 & \frac{1}{L} & -i_{\gamma 0} \\ 0 & 0 & 0 \\ 0 & 0 & 1 \end{bmatrix},$$

P_f is the number of pole pairs and J is the moment of inertia. Note that the subscript "0" indicates the value of the operating point in each variable.

Figure 3 shows the block diagram of the proposed V/f control for the grid-connection. The damping

control is used to the suppression of the torque oscillation due to the resonance between the moment of inertia and the armature inductance [1]-[4].

The following conditions are assumed in order to briefly discuss the stability and response.

(i) No-load condition: $\delta = 0$, $i_\gamma = 0$, $i_\delta = 0$

(ii) High-speed rotation condition

: $\omega_0 L >> R$, $\omega_0 L >> K_1 i_\delta$

(iii) The mechanical time constant is sufficiently larger than the electrical time constant: $p(\Delta i_\gamma) = 0$, $p(\Delta i_\delta) = 0$

(iv) The effect of HPF on stability is small.

The natural angular frequency ω_n and the damping factor ζ are calculated from the characteristic equation of the second-order system, which is derived by approximating the derived four-order state equation expressed as in Eq.(5) as a second-order system from the assumption of from (i) to (iv), and expressed as in (6) and (7),

$$\zeta = \frac{1}{2P_f}\sqrt{\frac{J}{L}}\cos\delta_0 K_1 \quad (6),$$

$$\omega_n = \frac{P_f \psi_m}{\sqrt{JL}} \quad (7),$$

where K_1 is the damping gain. As shown in Eq.(5), the damping factor ζ is the function of the feedback gain K_1. In other words, the proposed V/f control is stabilized by setting K_1 appropriately.

C. Output power control

Figure 4 shows the block diagrams of the output power controllers. Fig.4(a) shows the output power control by the virtual inertia. The state equation is same as Eq.(5) in the case of applying the virtual inertia. Thus, the output power control response is derived and agrees the approximated second-order system of PMSM. The natural angular frequency ω_n and the damping factor ζ are shown in Eq.(6) and Eq.(7).

Fig.4(b) shows the block diagram of the proportional output power control. The relationship between the torque of PMSM and the electric angular frequency is derived by ignoring a viscous resistance, and expressed as in (8),

$$p\omega = \frac{P_f}{J}(T - T_L) \quad (8),$$

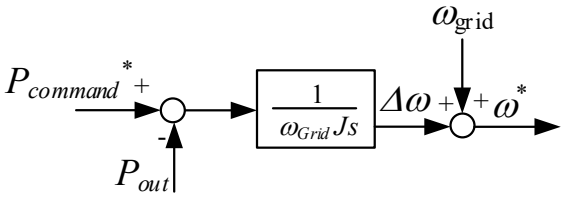

(a) The virtual inertia

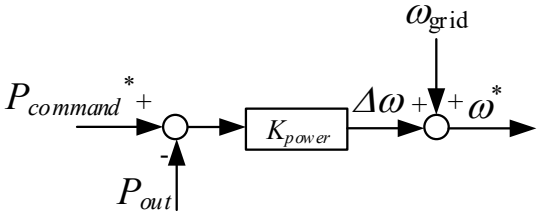

(b)The proportional control

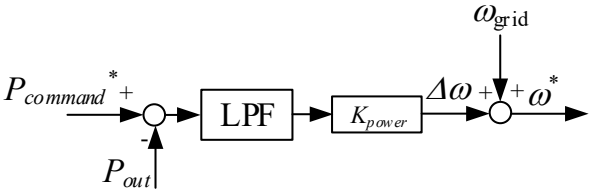

(c)The proportional control with LPF

Fig.4. The control diagram of the output power controller.

where T is the output torque and T_L is the load torque.

In the other hand, the relationship the output power of the proportional control and the electric angular frequency with the proposed V/f control is expressed as in (9),

$$\Delta\omega = K_{power}(P_{out} - P_{command}) = \frac{K_{power}}{\omega_{grid}}(T - T_L) \quad (9),$$

where K_{power} is the proportional gain of the output power control on the proposed V/f control and $P_{command}$ is the output power command. As shown Eq.(9), there is no the moment of inertia J in the proposed V/f control. Thus, The state equation of the grid-connected inverter does not include the moment of inertia J, and the state equation is derived by replacing J in Eq.(5). The way to replace J is derived by the relationship between Eq.(8) and Eq.(9), and expressed as in (10),

$$J = \frac{P_f}{pK_{power}\omega_{grid}} \quad (10).$$

The natural angular frequency of the grid-connected inverter ω_{n1} is calculated from the characteristic equation of the first-order system, which is derived by approximating the derived three-order state equation expressed as in Eq.(5)

and Eq.(10) as a first-order system from the assumption of from (i) to (iv), and expressed as in (11),

$$\omega_{n1} = \frac{P_f{}^2 \psi_m{}^2 K_{power} \omega_{grid}}{L} \quad (11).$$

In the grid-connected system with the proposed V/f control, the number of pole pair P_f is included the design of the proportional gain K_{power}. Thus, the natural angular frequency ω_{n1} is expressed as in (12),

$$\omega_{n1} = \frac{K_{power} V_{grid}{}^2}{2\omega_{grid} L} \quad (12).$$

The control response of the output power control without the damping control is expressed as in (13),

$$\frac{P_{out}}{P_{command}} = \frac{\omega_{n1}}{s + \omega_{n1}} \quad (13).$$

As shown in Eq.(13), there is no the oscillation occurs due to the resonance between the moment of inertia and the armature inductance. Fig.4(c) shows the block diagram of the proportional control with LPF used in Ref. [5]. The control response is derived by adding of LPF to Eq.(12) and expressed as in (14),

$$\frac{P_{out}}{P_{command}} = \frac{\omega_{LPF}\omega_{n1}}{s^2 + s\omega_{LPF} + \omega_{LPF}\omega_{n1}} \quad (14),$$

where ω_{LPF} is the cutoff angular frequency of LPF. The natural angular frequency ω_{n2} and the damping factor ζ are expressed as in (15) and (16),

$$\zeta = \frac{1}{2}\sqrt{\frac{\omega_{LPF}}{\omega_{n1}}} \quad (15),$$

$$\omega_{n2} = 2\zeta\omega_{n1} \quad (16).$$

In the comparison of each methods as shown as Fig.4, the control response should be second-order system by the disturbance suppression characteristics. However, the proportional output power control improves the disturbance suppression characteristics by the damping control. The control response by the adding the damping control to the proportional control is expressed as in (17),

$$\frac{P_{out}}{P_{command}} = \frac{s\omega_{n1} + \omega_{n1}\omega_{HPF}}{s^2 + s\left(\omega_{n1} + \omega_{HPF} - \frac{K_{HPF} V_{grid}}{\sqrt{2}\omega_{grid} L}\right) + \omega_{n1}\omega_{HPF}} \quad (17),$$

where ω_{HPF} is the cutoff angular frequency of the HPF and K_{HPF} is the damping gain with the proportional power control. In the case of the relationship between the angular frequency $\omega_{HPF} >> \omega_{n1}$, the control response of Eq.(17) is can be approximated to Eq.(14) by the parameter design, is expressed as in (18) and (19),

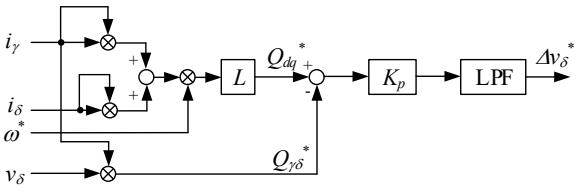

Fig.5 the control diagram of the high efficiency control.

Table 1 the simulation conditions.

Rated output power	P_{out}	1 kW
Grid-tied inductance	L	10 mH(%Z:24%)
Line resistance	R	0.2 Ω
Virtual inertia	J	0.08 kgm^2
Grid anguler frequency	ω_{grid}	314 rad/s
Grid maximum line-to-line voltage	V_{grid}	283 V
Damping factor	ζ	0.707
Natural anguler frequency	ω_n	14.2 rad/s

$$\zeta = \frac{1}{2\sqrt{\omega_{n1}\omega_{HPF}}}\left(\omega_{HPF} - \frac{K_{HPF} V_{grid}}{\sqrt{2}\omega_{grid} L}\right) \quad (18),$$

$$\omega_{n1d} = \sqrt{\omega_{n1}\omega_{HPF}} \quad (19),$$

where ω_{n1d} is the natural angular frequency of the proportional control with the damping control.

D. High efficiency control

Figure 5 shows the block diagram of the high efficiency control. The torque / current ratio is minimized by the $i_d = 0$ control with SPMSM. The $i_d = 0$ control is achieved indirectly by using the reactive power. In the dq-axis coordinate, the reactive power Q_{dq} is expressed as in (18),

$$Q_{dq} = v_q i_d - v_d i_q \quad (18).$$

In the steady state, the reactive power that assigned the voltage equation Eq.(1) is expressed as (19),

$$Q_{dq} = \omega\left\{L\left(i_d{}^2 + i_q{}^2\right) + \psi_m i_d\right\} \quad (19).$$

As shown Eq.(18), the reactive power that the $i_d = 0$ control is achieved is expressed as (20),

$$Q_{dq} = \omega L i_q{}^2 = \omega L I^2 \quad (20).$$

The reactive power in the γδ-axis coordinate $Q_{\gamma\delta}$ is expressed as in (21),

$$Q_{\gamma\delta} = v_\delta i_\gamma \quad (21).$$

Thus, the condition required for the $i_d = 0$ control is expressed as in (22),

$$\omega L\left(i_d{}^2 + i_q{}^2\right) = v_\delta i_\gamma \quad (22).$$

The function of the high efficiency control is the suppression the reactive power to zero. This function is same as the Q-V droop control.

Simulation results

Table 1 shows the simulation conditions. The control parameters are designed so that each

natural frequency ω_n, ω_{n1}, ω_{n2} and ω_{n1_d}, are equal. The output power command is a step command that changes to the rated output power P_{out} at t = 0. The ideal control response is designed to be a Butterworth filter of first-order and second-order system. The output power response by each output power control was checked to agree the ideal response.

Figuer 6 shows the output power response by each output power controls shown Fig. 4. Fig. 6(a) shows the response with the virtual inertia. The response with the virtual inertia is approximated to a second-order system by Eq.(6) and Eq.(7). From the simulation results, it is checked that the response agrees a second-order system. Fig.6(b) shows the response with the proportional control. The response with the proportional control is approximated to a first-order system as shown Eq.13. From the simulation results, it is checked that the response agrees a first-order system. However, the fluctuation of the grid frequency occurs on the output power. The cause of the fluctuation is a DC unbalanced current due to change in the voltage amplitude of the grid-tied inductor. The same fluctuation occurs when the power response is a second-order system. However, the effect of the fluctuation is large because the disturbance suppression characteristics of the proportional control is inferior than the one of the virtual inertia. Fig.5(c) shows the response with the proportional control with LPF. The response with the proportional control is approximated to a second-order system as shown Eq.14. From the simulation results, it is checked that the response agrees a second-order system. In addition, the similar response to V/f controlled virtual PMSM is obtained by the control parameter design of Eq.(15) and Eq.(16).

Figure 7 shows the frequency characteristic of the proportional power control with the damping control. The HPF cutoff angular frequency is set the 20 times of the angular frequency ω_{n1} designed by Eq.(12). From the comparison of the frequency characteristics, the response approaches the second-order system from the first-order system by the damping control. Fig.8 shows the response with the proportional control with the damping control. The response approaches from a first-order system to a second-order system. From the comparison with Fig.6(b), the fluctuation of the grid frequency is suppressed. The cause of the

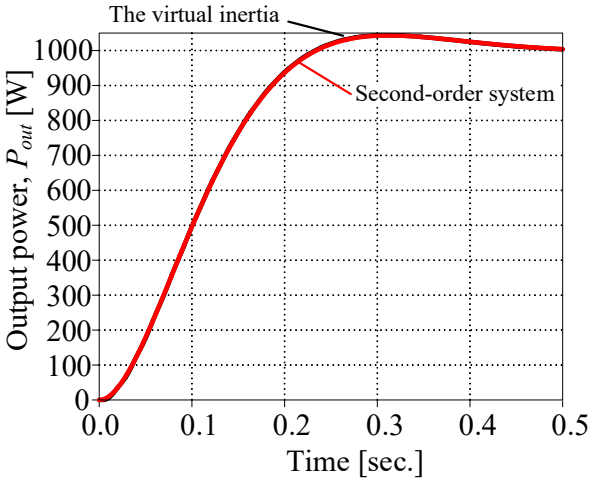

(a) The virtual inertia.

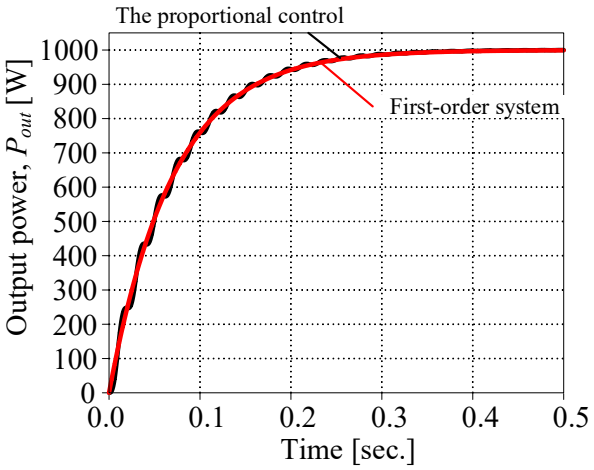

(b) The proportional control.

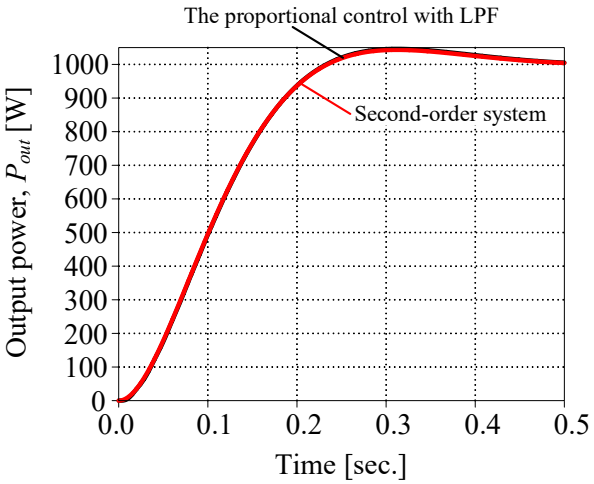

(c) The proportional control with LPF

Fig. 6 The output power control response.

suppression is the improving of the disturbance suppression characteristic by the damping control.

Figure 9 shows the dq-axis current response with the virtual inertia by the high efficiency control. The d-axis current is controlled to zero by the high efficiency control. Thus, the reactive power is suppressed to zero.

Conclusion

This paper discusses about the V/f controlled virtual PMSM for the grid-connection system. The output power response is designed to second-order system by the virtual inertia and the damping control. In addition, The second-order response is approximately obtained in the case of the proportional output power control is used with the damping control. In the future, the disturbance suppression characteristics will be evaluated for further improvement of the characteristics. Also, the output power response and the improving of the disturbance suppression characteristics will be confirmed by the experiment.

References

[1] J. Itoh, N. Nomura, and H. Ohsawa, “A comparison between V/f control and position-sensorless vector control for the permanent magnet synchronous motor”, PCC2002, pp.1310-1315, 2002.

[2] J. Itoh, T. Toi, M. Kato: "Maximum Torque per Ampere Control Using Hill Climbing Method Without Motor Parameters Based on V/f Control", 18th European Conference on Power Electronics and Applications (EPE'16), No. DS3d-Topic 4-0283, 2016

[3] J. Itoh, T. Toi, K. Nishizawa: "Stabilization Method Using Equivalent Resistance Gain Based on V/f Control for IPMSM with Long Electrical Time Constant", The 2018 International Power Electronics Conference, No. 23E1-5, pp. 2229-2236, 2018

[4] J. Itoh, T. Toi, K. Nishizawa: "Stabilization Method for IPMSM with Long Electrical Time Constant Using Equivalent Resistance Gain Based on V/f Control", IEEJ Transactions on Industry Applications, Vol. 8, No. 4, pp. 592-599 (2019)

[5] N. Pogaku, M. Prodanovic, and T. C. Green, “Modeling, analysis andtesting of autonomous operation of an inverter-based microgrid,” IEEETrans. Power Electron., vol. 22, no. 2, pp. 613–625, Mar. 2007.

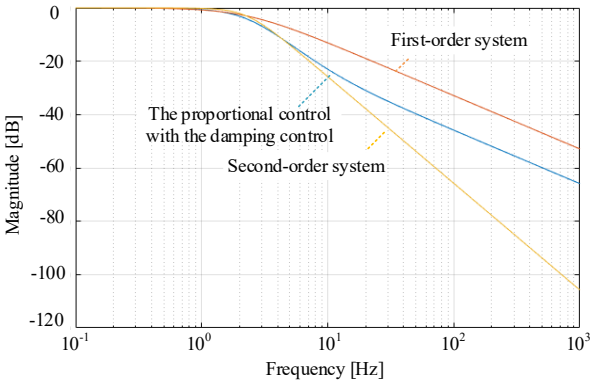

Fig. 7 The frequency characteristics of the proportional control with the damping control.

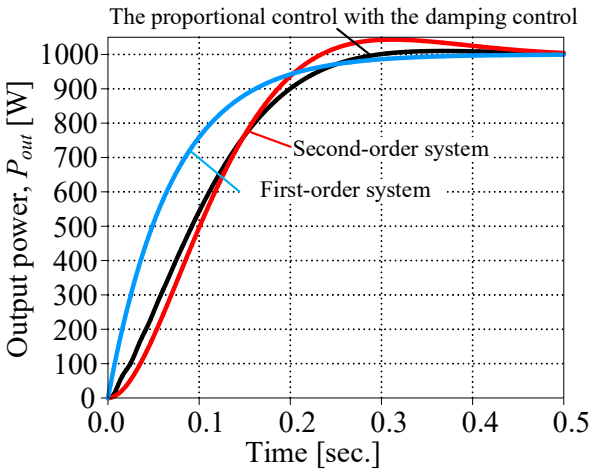

Fig. 8 The output power control response by the proportional control with the damping control.

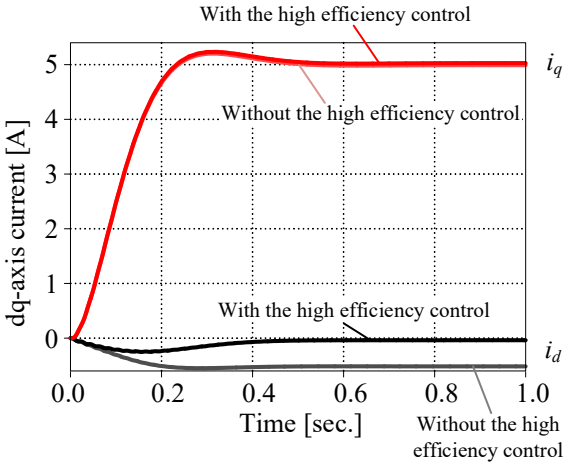

Fig. 9 The dq-axis current response by the virtual inertia with the high efficiency control.